

Conceptual design of extended magnetic probe set to improve 3D field detection in NSTX-U

S. Munaretto, E. J. Strait, M. J. Lanctot, and Z. R. Wang

Citation: [Review of Scientific Instruments](#) **89**, 10J108 (2018); doi: 10.1063/1.5036942

View online: <https://doi.org/10.1063/1.5036942>

View Table of Contents: <http://aip.scitation.org/toc/rsi/89/10>

Published by the [American Institute of Physics](#)

Articles you may be interested in

[Modal analysis of the full poloidal structure of the plasma response to \$n=2\$ magnetic perturbations](#)

[Physics of Plasmas](#) **25**, 072509 (2018); 10.1063/1.5029381

[Active spectroscopy measurements of the deuterium temperature, rotation, and density from the core to scrape off layer on the DIII-D tokamak \(invited\)](#)

[Review of Scientific Instruments](#) **89**, 10D110 (2018); 10.1063/1.5038349

[Relative intensity calibration of the DIII-D charge-exchange recombination spectroscopy system using neutral beam injection into gas](#)

[Review of Scientific Instruments](#) **89**, 10D116 (2018); 10.1063/1.5037333

[Helium line ratio spectroscopy for high spatiotemporal resolution plasma edge profile measurements at ASDEX Upgrade \(invited\)](#)

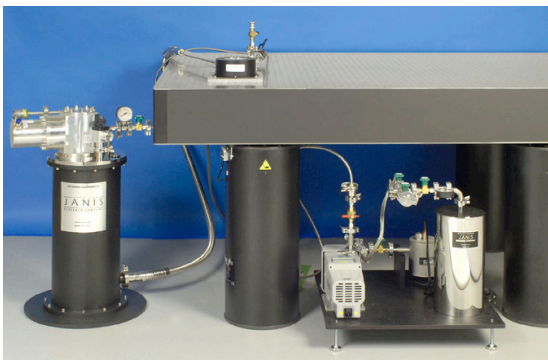
[Review of Scientific Instruments](#) **89**, 10D102 (2018); 10.1063/1.5034446

[Dynamic divertor control using resonant mixed toroidal harmonic magnetic fields during ELM suppression in DIII-D](#)

[Physics of Plasmas](#) **25**, 056102 (2018); 10.1063/1.5019777

[Particle and heat flux diagnostics on the C-2W divertor electrodes](#)

[Review of Scientific Instruments](#) **89**, 10J110 (2018); 10.1063/1.5038752



JANIS

Rising LHe costs? Janis has a solution.
Janis' Recirculating Cryocooler eliminates the use of Liquid Helium for "wet" cryogenic systems.

sales@janis.com www.janis.com **Click for more information.**

Conceptual design of extended magnetic probe set to improve 3D field detection in NSTX-U

S. Munaretto,^{1,a)} E. J. Strait,¹ M. J. Lanctot,^{1,b)} and Z. R. Wang²

¹General Atomics, San Diego, California 92121, USA

²Princeton Plasma Physics Laboratory, Princeton, New Jersey 08543, USA

(Presented 17 April 2018; received 19 April 2018; accepted 24 May 2018; published online 25 July 2018)

Adding toroidal arrays of magnetic probes at the top and bottom of NSTX-U would improve both the detection of the multimodal plasma response to applied magnetic perturbations and the identification of the poloidal structure of unstable plasma modes, as well as contribute to the validation of MHD models, improve the understanding of the plasma response to external fields, and improve the error field correction. In this paper, the linear MHD code MARS-F/K has been used to identify poloidal locations that would improve the capability to measure stationary or near-stationary 3D fields that may result from the plasma response to external sources of non-axisymmetric fields. The study highlighted 6 poloidal positions where new arrays of both poloidal and radial magnetic field sensors would improve the poloidal resolution. The proposed set of new arrays combined with the present ones is shown to be capable of measuring the poloidal structure of perturbations with $n \leq 6$ and of detecting the multimodal plasma response. Assessment of the trade-off in the poloidal length of the probes leads to an ideal length between 10 cm and 30 cm. A method to configure the probes of a toroidal array based on the singular value decomposition condition number is proposed, and an ideal solution and a low-cost one are presented. *Published by AIP Publishing.* <https://doi.org/10.1063/1.5036942>

I. INTRODUCTION

The measurement of quasi-stationary, non-axisymmetric (3D) magnetic fields is critical for NSTX-U.¹ It is required for example to understand the plasma response to external fields applied through two rows of 12 saddle coils dubbed Non-axisymmetric Control Coils (NCCs), to identify the poloidal structure of unstable plasma modes, to validate 3D perturbed equilibrium models as well as MHD stability models, to improve error field compensation, and to detect multimodal plasma response. Such measurements are challenging due to the typical small amplitude of the signal in tokamak plasmas ($\delta B/B \leq 10^{-4}$) and to the quasi-stationary nature of these fields. The work presented here is aimed at developing a conceptual design for an extension of the NSTX-U magnetic diagnostic system,² with the goal of more complete measurements of the non-axisymmetric 3D magnetic field. The study presented for NSTX-U is the first optimization of such a diagnostics for a spherical tokamak. Novel optimizations are presented, like that for the multimodal plasma detection and the reconfigurations of an existing set of probes, that can be applied to any other device. Extensive simulations of the plasma response to field applied through the NCCs using the linear MHD code MARS-F/K^{3,4} have been computed in order to predict the signal that can be detected by using magnetic sensors. The best

poloidal and toroidal distribution of sensors has been studied using the Singular Value Decomposition⁵ (SVD) condition number as a figure of merit. Unlike a conventional aspect ratio tokamak,⁶ the top and bottom parts of the machine were found to be the most important locations in which to install new toroidal arrays of magnetic probes. This paper will continue as follows: in Sec. II, the system of magnetic probes already installed in NSTX-U will be evaluated; in Sec. III, the optimal poloidal positions for new toroidal arrays are identified; in Sec. IV, the capabilities of the new system are evaluated; and in Sec. V, a study on the ideal length of the probes and a way to optimize their connection schemes are presented.

II. EVALUATION OF THE EXISTING SYSTEM

The existing system of magnetic probes to measure 3D fields is comprised of 3 toroidal arrays measuring the poloidal component of the magnetic field (B_p) and two toroidal arrays measuring the radial component (B_r). Two of the B_p and the B_r arrays are located in the low field side (LFS) of the machine, two above and two below the midplane, and have 12 probes each. A B_p array is located at the midplane in the high field side (HFS) and has 10 probes. The poloidal location of these arrays is indicated in black in Fig. 1. To evaluate the adequacy of the existing system to measure 3D fields, the SVD condition number is used, which gives an enhancement factor in the measurement error for poorly located probes. What has been found is that the toroidal distribution of the existing LFS arrays is sufficient to resolve toroidal harmonics up to $n = 5$, the HFS array up to $n = 4$.

Note: Paper published as part of the Proceedings of the 22nd Topical Conference on High-Temperature Plasma Diagnostics, San Diego, California, April 2018.

^{a)}Author to whom correspondence should be addressed: munaretto@fusion.gat.com

^{b)}Present address: DOE, Office of Fusion Energy Sciences, Washington, DC 20585, USA.

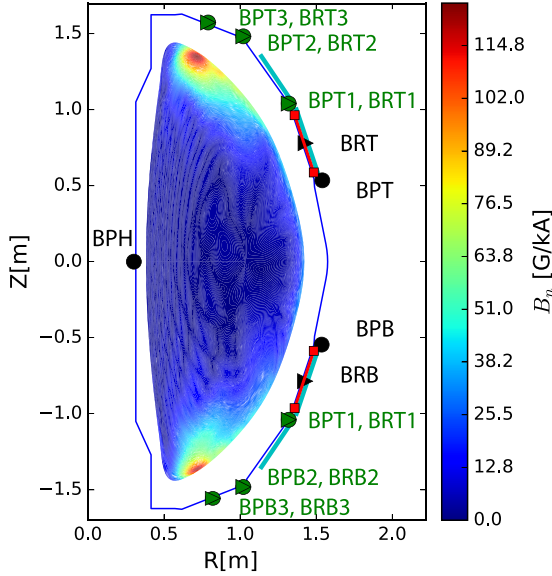


FIG. 1. Normal magnetic field computed by the MARS-F/K MHD code for an NSTX-U equilibrium at $\beta_N \sim 5.5$ and $q_{95} = 6.9$ when an $n = 2$ perturbation is applied with a phase difference of 72° between the upper and lower NCC rows. The contour plot corresponds to the sum of the vacuum and the plasma fields. In black are the sensor arrays already installed (circles are B_p sensors, triangles are B_r sensors); in green are the suggested locations for new sensors. The red squares connected by a solid line indicate the position of the NCCs, and the cyan solid lines indicate the position of conductive (passive) plates.

However, the poloidal distribution is insufficient to resolve local poloidal wavenumbers on either LFS or HFS of the device.

III. OPTIMIZATION OF NEW ARRAYS POLOIDAL LOCATION

To estimate the most relevant poloidal locations where additional toroidal arrays of magnetic probes would enhance the capability of the magnetic system, simulations of the plasma response to external perturbations with different toroidal periodicities ($1 \leq n \leq 3$) have been computed for two different ideal NSTX-U equilibria. In particular, one equilibrium is at high normalized plasma pressure ($\beta_N \sim 5.5$) and the other is at low normalized plasma pressure ($\beta_N \sim 2.5$). The MHD code used for the analysis is MARS-F/K. In Fig. 1, there is an example of the magnetic perturbation expected when the applied field couples strongly with the plasma.

Three key issues have been considered in order to identify the ideal positions for new toroidal arrays: the signal at the wall is strong enough to be measured; the new arrays allow the possibility to discriminate different poloidal wavelengths of the perturbation in different locations; it is feasible to install hardware in the selected location. Each of these issues is hereafter analyzed in terms of poloidal magnetic field.

A. Signal strength

The modeling suggests that the LFS has the most favorable locations for new arrays, in terms of signal strength. The strength of the signal at the wall has two main components, the vacuum contribution to the magnetic field and the plasma response to the applied field. What is of interest to be measured

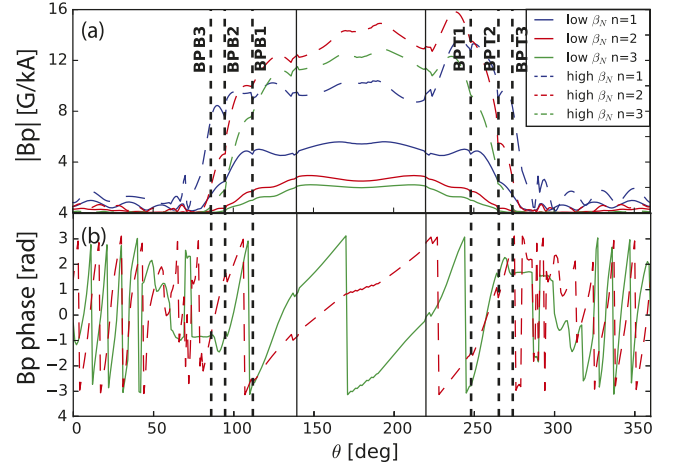


FIG. 2. Amplitude (a) and phase (b) of the poloidal component of the plasma response at the wall for different cases analyzed. In (b) only the highest and lowest amplitude case are reported. The vertical solid lines correspond to the existing probes; the dashed lines correspond to the suggested ones. The phase between the NCCs in the different cases is the one that produces the maximum response, so it varies case by case.

is the plasma contribution to the field, so the analysis has been focused on this component. In Fig. 2(a), the amplitude of B_p generated by the plasma at the wall (blue line in Fig. 1) is shown for the six cases analyzed (three toroidal periodicities of the perturbation for two different equilibria) as a function of the poloidal position θ at the wall. $\theta = 0^\circ$ corresponds to the HFS midplane, and $\theta = 180^\circ$ corresponds to the LFS midplane. The poloidal angle θ is calculated with respect to the magnetic axis position and goes counterclockwise. The solid vertical lines indicate the position of the existing B_p probes; the dashed lines indicate the position of the suggested new B_p arrays. The position of these is also shown by green symbols in Fig. 1. In general, the amplitude is weak in the region $\theta < 90^\circ$ or $\theta > 270^\circ$, i.e., the HFS, while it is stronger in the LFS. It is worth mentioning that the location in Fig. 1 where the perturbed magnetic field is the strongest is also the location where the wall is the farthest away from the plasma. Focusing on the proposed new arrays, the amplitude of the signal is greater than 1 G/kA of current in the NCCs for the probes dubbed BPT1 and BPB1. It decreases going toward the HFS, leaving the suggested probes BPT3 and BPB3 with a signal higher than 1 G/kA just for few cases.

B. Poloidal wavelength

Modeling suggests that the top and bottom of the device are the most interesting locations for new arrays also to study the poloidal structure of the plasma response. In fact, that is where the perturbation transitions from a long wavelength (LFS) to a short wavelength (HFS). Figure 2(b) shows the phase of the poloidal perturbation for two of the cases shown in plot (a), in particular the highest and the lowest amplitude case. For about $\theta < 50^\circ$ and $\theta > 320^\circ$, the wavelength of the perturbation is short in both the cases, while it is longer in the region $120^\circ < \theta < 240^\circ$ (approximately). The probes that are already installed provide a good picture of the modes in the LFS, while the single toroidal array in the HFS at $\theta = 0^\circ$ is not sufficient to identify the poloidal structure there.

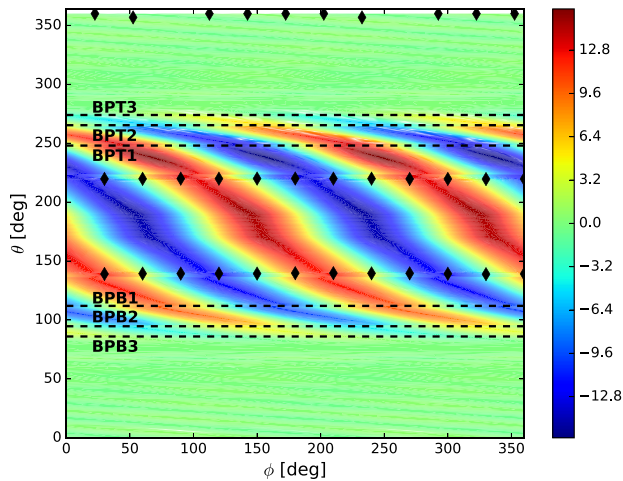


FIG. 3. Real part of the poloidal component of the field at the wall as a function of the poloidal and toroidal angle. The diamonds correspond to the position of the poloidal magnetic probes (B_p) already installed; the dashed lines correspond to the poloidal location where new B_p arrays are suggested. The equilibrium and the perturbation are the same as Fig. 1.

The new series of arrays is intended to measure the change in wavelength, being denser where the wavelength is shorter. The choice of the position for the suggested probes is clearer looking at Fig. 3. It shows the real component of the poloidal field expected at the wall for the case shown in Fig. 1. The x-axis is the toroidal direction; the y-axis is the poloidal one. The black diamonds represent the location of the existing poloidal probes; the dashed lines represent the poloidal position where new arrays are suggested. The figure highlights that in the region where the new arrays are suggested the perturbation has a change in poloidal wavelength λ_p , while its amplitude is still greater than a few Gauss. Figures 2 and 3 also show that for $n = 2$ the spacing between the poloidal locations is $\lambda_p/2$ or less, while even for $n = 3$ the spacing remains smaller than λ_p . Therefore, arrays at the proposed locations could resolve the detailed poloidal structure without spatial aliasing.

C. Hardware limitations and radial perturbation

The wavelength study presented in Secs. III A and III B suggests focusing on the top and bottom of the machine as well as the HFS. The latter though is not considered for the installation of new arrays due to the difficulty to install new hardware and the weak signal expected. The locations of interest left are therefore the top and bottom on the LFS. Here the positions of the arrays are constrained by conductive structures near the vessel and the predicted shortening of the wavelength; therefore, the six positions identified by the green circles in Fig. 1 are the best locations to install new arrays. Furthermore, a similar analysis to the one presented has been carried out for the radial component of the field. Good positions for radial probes are similar to those for the poloidal probes.

IV. CAPABILITY OF THE NEW SYSTEM

Although the poloidal locations of the proposed 3D magnetics are optimized to detect the poloidal structure of 3D

fields with toroidal periodicity $n \leq 3$, the possibility to measure the plasma response to external perturbation with toroidal periodicity up to $n = 6$ (limit of the NCCs) and to identify a multimodal plasma response is highly desirable. Both the possibilities are hereafter analyzed.

A. Plasma response to $n > 3$ perturbations

Simulations of the plasma response to external perturbations with toroidal periodicity $4 \leq n \leq 6$ with the MARS-F/K code have been performed for the same equilibria of Sec. III. For the low β_N case, the signal at the wall is lower than 1 G/kA all along the wall for both the poloidal and the radial component. The poloidal component of the plasma response at the wall in the high β_N case is shown in Fig. 4, where (a) is its amplitude, and (b) is its phase. The horizontal axis follows the same convention as Fig. 2. As expected, the field at the wall for $n > 3$ is smaller than for $n \leq 3$, but the general poloidal structure is similar, with a stronger field in the LFS between the NCCs and a much lower field in the HFS. Panel (b) also highlights that the proposed positions in addition to the present arrays are located in an optimal position to detect the change in wavelength between the LFS and the HFS. As for $n \leq 3$, the BPT and BPB probes are in a long wavelength region and BPT1 and BPB1 are in the transition region. Probes BPT2, BPB2, BPT3, and BPB3 are located in the shortened wavelength region. In conclusion, when the signal at the wall is strong enough to be detected, the poloidal position suggested for the toroidal arrays to detect the plasma response to $n \leq 3$ perturbations is a good position also for perturbations with $3 < n \leq 6$ considering the hardware limitations.

B. Detection of multimodal plasma response

Recent studies in DIII-D showed the presence of a multimodal plasma response to $n = 2$ external perturbations depending on the poloidal spectrum of the applied field.⁷ In these studies, it was observed that the amplitude of the B_p field measured in the HFS had a different dependence on the phasing between the coils used to apply the perturbation than in the LFS, indicating the presence of at least two independent,

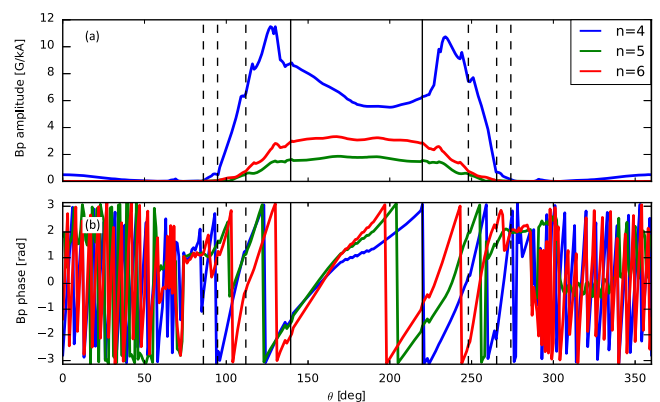


FIG. 4. Poloidal distribution of the poloidal magnetic field at the wall for the high β_N case with applied perturbations with toroidal mode numbers $n = 4$, $n = 5$, and $n = 6$. The figure shows the amplitude of the field (a) and the phase (b). The vertical dashed lines indicate the position of the suggested new arrays; the solid lines indicate the position of the already installed arrays.

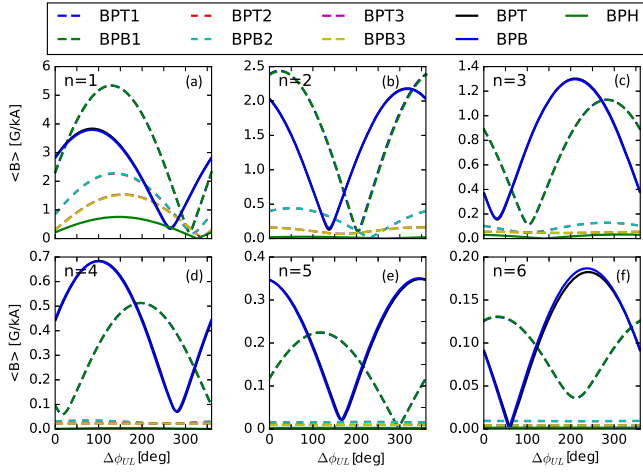


FIG. 5. Multimodal plasma response for the low β_N case as a function of the NCC phasing. Each panel corresponds to a different toroidal perturbation applied, different line style and color used to identify different toroidal arrays.

stable modes with different couplings to the non-axisymmetric coils. Therefore, the dependence of the amplitude of the measurements by the poloidal field probes as a function of the NCC phasing is used as a parameter to assess the possibility to identify the multimodal plasma response. In Fig. 5, each panel represents the plasma response measured by using the sensors as a function of the phasing of the NCCs. In each panel, a different toroidal periodicity, from $n = 1$ to $n = 6$, is shown, for the low β_N case. The different curves are the nine different arrays of B_p probes, including the existing LFS and HFS arrays as well as the six proposed arrays. Two important observations can be made from this figure: 1—for each toroidal periodicity there are at least 2 arrays with clearly different dependences on the poloidal structure of the applied field and 2—adding the toroidal arrays called BPT1 and BPB1 to the already installed BPT and BPB arrays is enough to detect the presence of a multimodal plasma response for this equilibrium.

V. OPTIMIZING THE SYSTEM

In this section, some considerations about the poloidal length of the probes and how to connect them in order to measure the small 3D signals are presented.

A. Probe length

Neglecting all the hardware limitations, the size of a probe is constrained by two main factors: it has to be small enough to detect spatial variation of the magnetic field and at the same time big enough to acquire a detectable signal. The signal coming from a Mirnov coil is $V_{\text{coil}} = NA \, d\langle B \rangle_{\text{Volume}}/dt$, where N is the number of turns the probe is comprised of, A is the area of the probe, and $\langle B \rangle$ is the average magnetic field inside the probe. The signal acquired after the integration becomes $V_{\text{integrated}} = G NA \langle B \rangle_{\text{Volume}}(t)$, with G being a constant related to the integrator. Since we are looking at the poloidal length, the area of the probes is assumed to be fixed, as well as the integrator features. This leaves two quantities of interest: $\langle B \rangle$

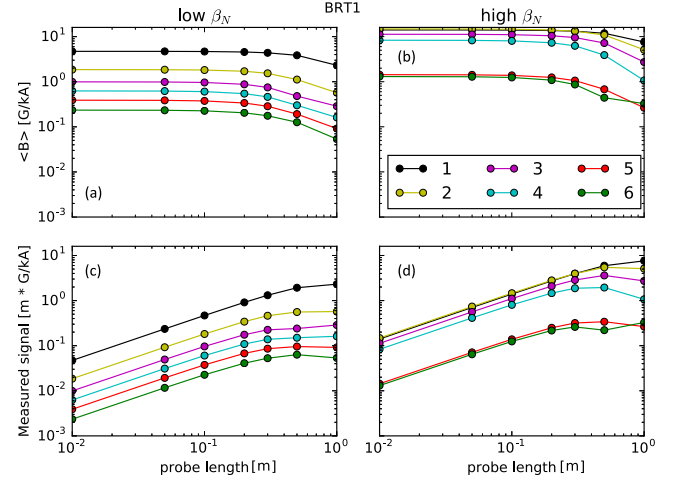


FIG. 6. Size scan for B_r probe in the toroidal array BRT1. In (a) and (b), the field measured by such array as a function of the probe size; in (c) and (d), a quantity proportional to the voltage measured again as a function of the probe size. (a) and (c) are the results for the equilibrium with $\beta_N \sim 2.5$; (b) and (d) are the results for the equilibrium with $\beta_N \sim 5.5$. The different colors correspond to different toroidal periodicities (n) applied.

and $\text{length} \times \langle B \rangle$ since the length is proportional to the number of turns N . The results of the scan of possible lengths from 1 cm to 1 m for the probe BRT1 are shown in Fig. 6. Panels (a) and (b) correspond to $\langle B \rangle$ measured in the low β_N and high β_N case, respectively. Panels (c) and (d) show the same results multiplied by the poloidal length of the probe. The x-axis in all the plots is the length of the probe, the different colors correspond to the toroidal periodicities. Looking at the magnetic field, panels (a) and (b) suggest that probes between 1 cm and 10 cm in length will measure a comparable $\langle B \rangle$, while bigger probes will measure a smaller averaged magnetic field. Looking at the detected signal, panels (c) and (d) show that increasing the size of the probe up to 30 cm the detected signal also increases, while probes greater than 30 cm do not always have an improved detected signal, like for example for $n = 2$ in panel (c) and $n = 4$ in panel (d).

Figure 7 is similar to Fig. 6, but in this case a probe measuring the poloidal field in a location where the perturbation

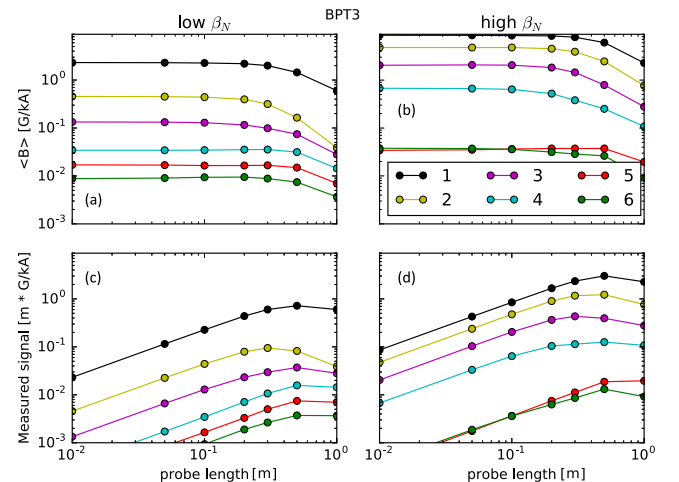


FIG. 7. Similar to Fig. 6 but for a probe in the BPT3 array.

is expected to have a short wavelength is considered (BPT3). The figure shows results similar to those for BRT1. Summarizing, these results suggest that the ideal length of the probes to detect perturbations with $n \leq 6$ is between 10 cm and 30 cm, where the smaller lengths enable more precise identification of the poloidal structure, while the larger lengths will have a larger signal. An extra note is that among the limitations neglected there is also the distance between the arrays. For example, the two topmost arrays are about 25 cm apart so that 30 cm long probes in both the arrays are not desirable for good spatial resolution.

B. Connection scheme

Connecting the sensors in pairs and digitizing the difference eliminate the contribution from the strong axisymmetric field in order to improve the resolution and signal to noise ratio of the measurement. A method to optimize the connection scheme is hereafter discussed. To compare different sets of magnetic sensor pairs, the condition number of the basis matrix is used as a figure of merit.⁸ A well-conditioned matrix has a low condition number (ideally 1), while the uncertainty in detection or rejection of the specified set of modes increases in proportion to the condition number. The robustness of a given set of sensor pairs to the loss of a single sensor has been used as a secondary figure of merit. It is represented by the largest condition number that results from omitting any single sensor in the original array. The assessment then aimed to minimize K_0 and K_1 , where K_0 is the condition number for the complete set and K_1 is the condition number for the worst-case loss of one sensor. For a typical array of 12 sensors, the number of possible sets of 12 pairs of sensors is too large to catalog and test all of them. Therefore, a Monte Carlo method was used, in which sets of pairs are selected randomly, with the constraints that each sensor should be a member of no more than two pairs. An optimized set of 12 pair connections is illustrated in Fig. 8(a), where the squares correspond to the toroidal distribution of the probes of the existing LFS toroidal arrays. For this case, $K_0 = 1.2$ and $K_1 = 2.3$. A low-cost alternative to a full toroidal array is a reduced set of sensors designed to detect just a single toroidal mode number, rather than simultaneous detection of several toroidal modes. The

capability of such configuration is limited. Because different mode numbers cannot be discriminated, this approach is suitable only when a single toroidal mode number is known to be dominant. Figure 8(b) shows a configuration of 4 sensor pairs that is optimized for low K_0 in single-mode detection of $n = 1$, $n = 2$, or $n = 3$, for the existing probes in the HFS.

VI. CONCLUSIONS

In this study, it is shown that the addition of 12 toroidal arrays of probes equally distributed between the top and the bottom of the machine as well as between poloidal and radial sensors would provide adequate measurements to discriminate the poloidal structure of 3D fields up to $n \leq 6$. It is also shown that adding only 4 new probes between the passive plates either on the top or on the bottom of the machine would allow us to identify the existence of a multimodal plasma response in the case of a known single toroidal periodicity. A large variety of options between these two extremes are available.

ACKNOWLEDGMENTS

The authors wish to thank S. Gerhardt, R. J. La Haye, Y. Q. Liu, L. Morton, C. Myers, J.-K. Park, and S. A. Sabbagh for the useful conversations and their help. This work was supported by U.S. DOE under Nos. DE-FC02-04ER54698, DE-FG02-99ER54522, and DE-AC02-09CH11466. The digital data for this paper can be found at <http://arks.princeton.edu/ark:/88435/dsp011v53k0334> and <https://fusion.gat.com/global/D3D.DMP>.

This report was prepared as an account of work sponsored by an agency of the United States Government. Neither the United States Government nor any agency thereof, nor any of their employees, makes any warranty, express or implied, or assumes any legal liability or responsibility for the accuracy, completeness, or usefulness of any information, apparatus, product, or process disclosed, or represents that its use would not infringe privately owned rights. Reference herein to any specific commercial product, process, or service by trade name, trademark, manufacturer, or otherwise, does not necessarily constitute or imply its endorsement, recommendation, or favoring by the United States Government or any agency thereof. The views and opinions of the authors expressed herein do not necessarily state or reflect those of the United States Government or any agency thereof.

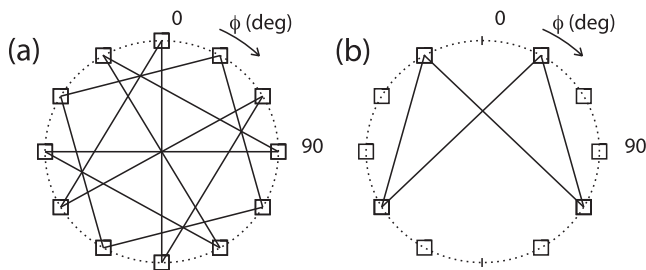


FIG. 8. (a) Optimized set of 12 pair connections for detection of $n \leq 3$ with the existing LFS arrays. (b) Optimized set of 4 pair connections for single-mode detection ($n = 1$ or $n = 2$ or $n = 3$) for the existing HFS array.

¹J. E. Menard *et al.*, *Nucl. Fusion* **52**, 083015 (2012).

²S. P. Gerhardt *et al.*, *Rev. Sci. Instrum.* **85**, 11E807 (2014).

³Y. Q. Liu *et al.*, *Phys. Plasmas* **7**, 3681 (2000).

⁴Y. Q. Liu *et al.*, *Phys. Plasmas* **15**, 112503 (2008).

⁵W. H. Press, S. A. Teukolsky, W. T. Vetterling, and B. P. Flannery, *Numerical Recipes in C: The Art of Scientific Computing* (Cambridge University Press, 1988).

⁶J. D. King *et al.*, *Rev. Sci. Instrum.* **85**, 083503 (2014).

⁷C. Paz-Soldan *et al.*, *Phys. Rev. Lett.* **114**, 105001 (2015).

⁸E. J. Strait *et al.*, *Rev. Sci. Instrum.* **87**, 11D423 (2016).